European Journal of Pharmaceutics and Biopharmaceutics 74 (2010) 26–32

Contents lists available at ScienceDirect

European Journal of Pharmaceutics and Biopharmaceutics

journal homepage: www.elsevier.com/locate/ejpb

Research paper

Photothermal imaging in 3D surface analysis of membrane drug delivery

B. Gotter [a,*], W. Faubel [b], R.H.H. Neubert [a,c]

[a] Institute of Pharmacy, Martin Luther University, Halle/Saale, Germany
[b] Institute of Functional Interfaces, Karlsruhe Research Centre, Karlsruhe, Germany
[c] Institute of Applied Dermatopharmacy, Martin Luther University, Halle/Saale, Germany

ARTICLE INFO

Article history:
Received 23 December 2008
Accepted in revised form 22 May 2009
Available online 29 May 2009

Keywords:
Photothermal deflection spectroscopy
Photothermal imaging
Depth profiling
Drug penetration
Bovine hoof
Methyl orange
Dithranol

ABSTRACT

Various methods exist for research into the penetration process in the human nail plate and for investigation of dermal drug delivery. Application of spectroscopic methods in this scientific field is gaining importance. However, no method meets all demands of the large variety of applications. An alternative optical technique for the characterisation of samples is the photothermal spectroscopy. Photoacoustic techniques, photothermal radiometry, and photothermal beam deflection spectroscopy (PDS) are non-destructive analytical techniques that take advantage of the so-called photoacoustic and photothermal phenomena. PDS, in conjunction with an appropriate scanner, allows for depth profiling and is a promising technique for studies of three-dimensional drug diffusion into artificial and biological membranes. The objective of this article is to demonstrate the use of PDS imaging for pharmaceutical applications and drug delivery studies, with two experiments being used as examples: the follow-up of lateral dithranol penetration into an artificial membrane and depth-resolved measurement of the distribution of a model drug within a keratin membrane from bovine hoof.

1. Introduction

The human skin is an extraordinarily complex organ that consists of several layers assuming multiple functions. On the one hand, the skin protects the organism from exhaustive water and heat loss. On the other hand, barrier functions protect against the penetration and permeation of microorganisms and toxins into the organism. This is one of the main tasks of the outermost layer of the skin, which is known as the horny layer or the stratum corneum (sc). The sc is a heterogeneous membrane that is composed of keratin-rich corneocytes embedded in a lipid matrix. The so-called "brick and mortar" model represents an effective barrier that inhibits not only toxins and microorganisms, but also pharmaceutical agents from penetrating the skin. In addition, the human nail, which is an adnexa of our skin, fulfils barrier and protection functions. However, there are various types of skin diseases and infections affecting our barrier regions. As the transport of specific drugs into deeper layers and particularly where the permeation is desired, the human nail, the epidermis, and especially the sc have been investigated with respect to their composition and manipulation of the penetration process for years. The optimisation of pharmaceutical formulations in terms of drug delivery and skin penetration is a major challenge in dermatopharmacy. A number of in vitro methods exist for studying penetration into the human nail plate [1–3] and for investigating dermal drug delivery [4]. The spectroscopic methods, including FTIR–ATR (Fourier transform infrared–attenuated total reflection) [5–7], FTIR–PAS (Fourier transform infrared–photoacoustic spectroscopy) [7–9], FT-Raman (Fourier transform-Raman) [10], and CRM (confocal Raman microspectroscopy) [11–14], offer certain advantages. In particular, the analyte can be determined with minimal or no sample preparation required. Furthermore, extraction steps are omitted. This simplification of the analytical procedure significantly increases the reproducibility of the analysis. Furthermore, on-line spectroscopic measurements permit the kinetics of reactions to be followed. However, no method meets all demands of the large variety of samples. In particular, FTIR and Raman spectroscopy are suited to only limited investigation of opaque samples, while FTIR–PAS is capable of measuring such substances. However, this technique is sensitive to disturbing noise. An alternative optical technique for the characterisation of samples is photothermal spectroscopy. Photoacoustic techniques [15], photothermal radiometry, and photothermal beam deflection spectroscopy (PDS) [16,17] are non-destructive analytical techniques that take advantage of the so-called photoacoustic and photothermal phenomena. In the past years, inexpensive and non-destructive variants of photothermal spectroscopy were developed successfully. The so-called OTTER (optothermal transient emission radiometry) technique is a photothermal technology that yields a set of insights into skin research. The measuring principle is

* Corresponding author. Institute of Pharmacy, Division Pharmaceutics and Biopharmaceutics, Martin Luther University, Wolfgang-Langenbeck-Str. 4, 06120 Halle/Saale, Germany. Tel.: +49 345 5525214.
E-mail address: bernhard.gotter@pharmazie.uni-halle.de (B. Gotter).

0939-6411/$ - see front matter © 2009 Elsevier B.V. All rights reserved.
doi:10.1016/j.ejpb.2009.05.014

slightly different from that of PDS. The sample is excited by an incident beam and the transient thermal emission is collected by a conventional MCT (mercury cadmium tellurite) detector. Depth profiling is accomplished by recording time-resolved spectra. It is based on time-dependent changes of the thermal emission decay signal, as the heat diffuses into the sample [18]. Depth distribution of water and ethylene glycol in the horny layer was measured successfully down to 10 μm penetration depth [19]. However, this promising technique regrettably has some limitations. IR radiation that does not come from the sample cannot be distinguished from the heat radiation originating from the sample of interest. Radiation coming from deeper layers of a sample decreases rapidly below the detection limit of the MCT detector. For this reason, depth profiling is restricted to a few microns.

The photothermal beam deflection spectroscopy (PDS) was first developed in 1980 [20,21]. Variants have been used for a wide range of spectroscopic and imaging applications. Photothermal imaging for monitoring short-term nanoscale thermal effects in living cells was evaluated by Lapotko et al. [22,23]. However, PDS is an appropriate imaging tool not only on the nano scale, but also at higher orders of magnitude. Koebel et al. introduced a type of series PDS imaging for probing protein arrays [24].

PDS, in conjunction with an appropriate scanner and depth profiling, is a promising technique for studies of three-dimensional drug diffusion into artificial and biological membranes. The combination of lateral imaging and depth-resolved measurements allows for a 3D visualisation of a sample. Results regarding the potential use of the non-invasive method of photothermal beam deflection in pharmaceutical research, together with preliminary results obtained by our group for lateral drug diffusion in an artificial membrane, are published in [25]. According to Hanh et al., PDS is highly sensitive to drug penetration. The fact that only a minimum sample preparation is needed and no substances (e.g. fluorescent compounds or gold nanoparticles) have to be added makes this spectroscopic technique advantageous. However, Hanh's work only covers the lateral (x, y dimension) and not the z dimension of drug penetration. The work presented here will focus on this latter aspect of depth profiling (x, y, and z dimensions), the final objective being to obtain a complete picture of the penetration process of drugs into a tissue. Use of PDS imaging for pharmaceutical applications and drug delivery studies will be illustrated with two experiments: the temporal follow-up of dithranol (DI) penetration into an artificial membrane and depth-resolved measurement of the distribution of a model substance, methyl orange (MO), within a keratin membrane from bovine hoof.

2. Materials and methods

2.1. Method

The experimental setup of the PDS and the non-destructive evaluation of thermal properties were discussed in detail previously [17]. Now, the photothermal principles will be described briefly. Periodic heating by a modulated pump beam produces periodic heating of the air adjacent to the sample surface as a consequence of heat transfer from the sample surface. This causes periodic variations of the index of refraction, n, of air. This temperature-dependent density oscillation in the air is monitored locally with a probe laser beam which skims along the surface of the sample and through the heated region (Fig. 1). Periodic deflections of this probe beam due to the refractive index gradient are measured by a position-sensitive optical detector. Detection is made on a line l along the path defined by the illuminated region of the surface. l is the interaction pathway between the probe beam and the temperature gradient [21].

The angle of deflection ϕ from the original trajectory is given by

$$\phi = -\int_P \left(\frac{1}{n}\right) * \left(\frac{dn}{dT}\right) * \nabla T_g \times dl \tag{1}$$

where n is the gas (air) index of refraction and dn/dT is the temperature gradient of the index of refraction. T_g is the periodic temperature distribution in the air. P is the probe beam interaction path and dl is an incremental distance along P [26]. With regard to the sample, there are three important parameters. They are the sample thickness d, the optical absorption length $1/\beta$, where β is the absorption coefficient in cm^{-1}, and the thermal diffusion length μ, which determines how far a periodic heat wave can travel in a solid before dissipating. The thermal diffusion length is

$$\mu = \sqrt{\frac{\alpha}{\pi f}} \tag{2}$$

where α is the thermal diffusivity of the sample

$$\alpha = \frac{k}{\rho C} \tag{3}$$

(k = thermal conductivity, ρ = density, and C = specific heat) and f is the frequency of the heat wave, in this case, the frequency at which the excitation beam is chopped. This means that at high frequencies, when the thermal diffusion length is smaller than the optical absorption length, only small thermal diffusion layers can be studied at the sample surface. At lower modulation frequencies, by contrast, thermal diffusion length increases and light absorption in deeper layers can be studied. Provided that the thermal diffusivity (Eq. (3)) of the sample of interest is known, a modulation of the excitation frequency permits several levels of sample depth to be studied (Eq. (2)).

The membranes used for the following experiments are highly transparent for the laser excitation wavelength. In this case, the optical absorption length is much higher than the thermal diffusion length. Thermal distribution agrees with the intensity distribution of the laser profile. If the operating mode of the laser is TEM_{00}, the beam intensity shows a Gaussian profile and the heat diffuses in cylindrical form along the pump beam within the kera-

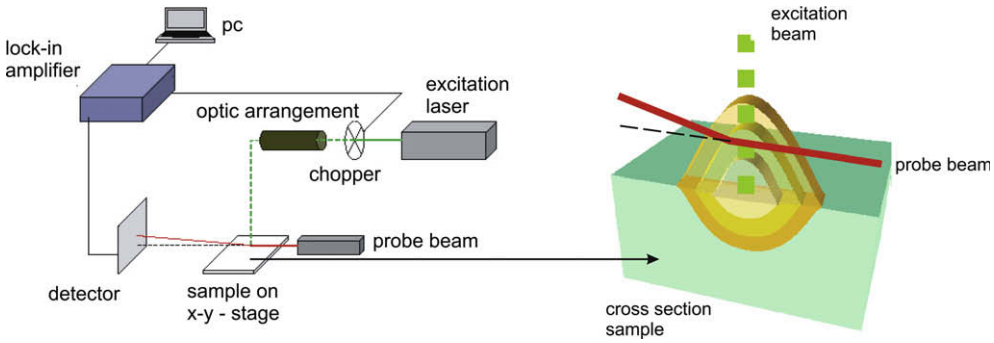

Fig. 1. Layout of the photothermal device (left). Schematic of the probe beam deflection process, as the beam is passing the thermal lens at the measurement point.

tin membrane. At the surface, the heat enters the adjacent gas phase, giving rise to the thermal lens. The thermal lens results from the heat generated at a sample depth $d \leqslant$ thermal diffusion length μ only. Since the membrane material does not generate significant PDS signals, penetrating substances which absorb the excitation radiation can be detected.

3. Experimental

All PDS measurements were performed with a photothermal device (Monobloc Phototherm Dr. Petry, Saarbruecken, Germany) by means of deflection detection of the oscillating surface temperature (Fig. 1). A diode-pumped frequency-doubled Nd:YAG laser (wavelength: 532 nm; 100 mW, 10 mW of which hit the sample, B&W TEK, Newark, DE, USA) operating in the TEM_{00} mode was utilised as excitation source. The incident heating beam was modulated by a mechanical chopper (model NFO-3501, New Focus, San Jose, CA, USA). The probe beam (HeNe laser wavelength λ = 633 nm, 1 mW; JDS uniphase model 1101P, Montea, CA, USA) deflection amplitude (PDS signal) was detected by a four-quadrant position-sensitive detector (Hamamatsu, Japan) and processed by means of a lock-in amplifier (model 5210, EG&G, Princeton, NJ, USA). The probe beam deflection consists of two mechanisms, namely, the normal component ϕ_n and the transverse component ϕ_t. In the following experiments, the amplitude of ϕ_t was used to detect the beam deflection. For scanning purposes, an XY translation stage (Limes 90, OWIS, Staufen, Germany) was used, allowing for moving the sample with a step accuracy of 1 µm.

3.1. 3D imaging of drug distribution

A keratin membrane from bovine hoof was applied as acceptor and attached to a flow-through chamber. Bovine hoof membranes can be used as a nail model for penetration and permeation experiments. The structure of bovine hoof equals that of human nails [2]. A 55 µm thick membrane was taken from the distal part of the ball horn by a microtome. The circular area of contact between the membrane and the donor was 12.5 mm^2. The donor was a solution composed of the model substance methyl orange (MO) 0.1% (w/w) and glycerine 6% (v/v) in phosphate-buffered saline of pH 7.4. This solution was passed through the chamber (chamber volume = 31.25 mm^3) for 90 min at a constant flow rate of 4.95 ml/h by a syringe pump (Razel Scientific Instruments, Stamford CT USA). The pure solvent was used for saturation of the hoof membrane directly before the solution was allowed to contact the membrane. A diode-pumped frequency-doubled Nd:YAG laser was utilised as excitation source and an HeNe laser served as probe laser. Fig. 2b shows the absorption spectrum of visible radiation of the donor solution (measured with BTC 112E CCD Array Spectrometer, B&WTEK, Newark, DE, USA). Methyl orange [sodium-4-(dimethylamino)-azobenzene-4′-sulphonic acid] was chosen as a model drug, since the wavelength of the excitation source used matched the absorbing spectral region, while the pure hoof membrane did not show any significant absorption in the visible spectrum. In this way, selective determination of the model drug in the membrane was possible. Upon the completion of the flow process, the membrane was removed and dried in a low-humidity environment (<30% rH). Afterwards, the membrane was attached to an adhesive tape on a metal sample holder (Fig. 1). In order to measure a representative part, an area (1 mm × 2 mm) containing both a region with penetrated drug and a non-influenced part was analysed at 14, 26, 31, 36, 41, and 46 Hz modulation frequencies.

3.2. Imaging of lateral penetration

The same photothermal device as that mentioned before was used for imaging of the lateral penetration. A semi-solid suspension which contained 10% dithranol (1, 8-dihydroxyanthrone) (DI) in white soft paraffin was used as the donor phase and a DDC membrane [27] (thickness 28 µm) served as acceptor (Fig. 3). The Nd:YAG laser was applied for the excitation of the sample and an HeNe laser was used as the probe beam. For this experiment, a frequency of 26 Hz was chosen to modulate the excitation beam. In order to observe the lateral diffusion of the drug, an area of 1 mm × 0.75 mm was measured in front of the applied formulation, such that the probe beam position was parallel to the boundary edge of the applied formulation (Fig. 3). The imaging field contained 1435 equidistant measuring points, resulting in a lateral resolution of 25 µm × 25 µm. A PDS image took 17 min to be recorded. In order to avoid disturbing effects of the formulation on the probe beam pathway, the imaging area was 250 µm away from the suspension. Imaging measurements were carried out 2.5, 5.5, 25.5, 35.5, 45.5, and 55.5 h after starting the experiment.

4. Results and discussion

4.1. Imaging of lateral drug penetration

The preliminary experiment performed by Hanh et al. [21] shows a single image of the dithranol distribution in a DDC membrane. In our experiment, studies were extended to also cover the

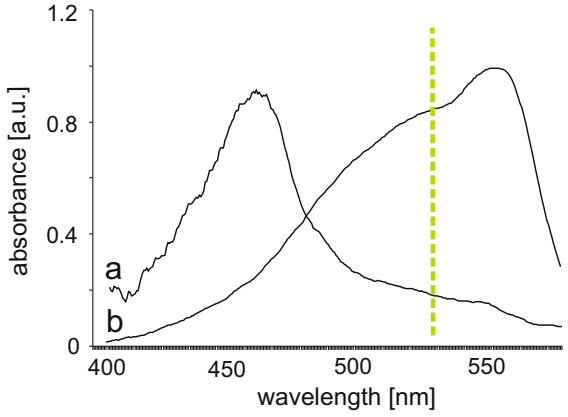

Fig. 2. Absorbance spectra in the visible region (400–600 nm) of (a) dithranol and (b) methyl orange. The dashed line indicates the wavelength of the Nd:YAG laser (532 nm) used as excitation beam.

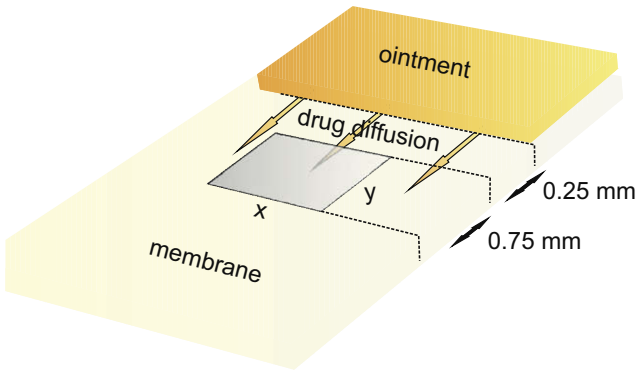

Fig. 3. Schematic of the lateral DI diffusion experiment. The formulation (donor) is located at the top of an artificial DDC membrane (acceptor). The area for PDS imaging is 250 µm distant from the formulation to avoid any kind of interaction of the probe beam and formulation.

temporal monitoring of dithranol diffusion. In order to achieve a higher sensitivity, the wavelength of excitation of 1064 nm was adapted to 532 nm using a frequency-doubled Nd:YAG laser.

As shown in Fig. 2a, the wavelength of the excitation beam does not hit the absorption peak of DI at the maximum, but the absorbed energy is sufficient to reach a selective excitation. The results of PDS imaging of dithranol (DI) diffusion into the artificial DDC membrane are depicted in Fig. 4. A selective determination of drug distribution within the artificial membrane was possible, since pure DDC membrane does not absorb radiation in this spectral region. The diffusion process was observed for 55 h. The PDS images in Fig. 4a and b exemplify the expansion of the drug in the DDC membrane. The measurement made 2.5 h after the formulation had been applied shows a homogeneous PDS signal distribution, whereas significantly increasing PDS signals were detected 55 h after application. As expected, a gradient of the PDS signal was observed. By incremental diffusion way, the drug concentration within the membrane was ascending with lower velocity. The highest DI content was determined near the ointment. Fig. 4c provides a more detailed view of a single line of the image, which is indicated by the red line in Fig. 4a. Based on the imaging data, the PDS signal to distance profile can be studied at each line or even at a single point. The increase in the PDS signal versus time is presented for three measurement points that are located along the line mentioned above (Fig. 4d). These points represent the shortest, longest, and medium distance to the drug reservoir, as indicated in Fig. 4d. As expected, the slope of the curve increases with decreasing distance. Furthermore, the imaging technique reveals that the drug is distributed with a heterogeneous front. Highest PDS signals were found in the peripheral regions adjacent to the formulation (Fig. 4b). This behaviour is caused by a heterogeneous distribution of the DI particles in the donor suspension. The artificial acceptor membrane possibly does not provide constant conditions all over the sample.

4.2. Imaging of 3D drug distribution

The PDS technique can not only be used for lateral imaging, but it is also possible to pursue drug distribution perpendicular to the surface.

Two types of photothermal visualisation exist (Fig. 5). The *x*-axis and *y*-axis indicate the scanned area. The intensity of the PDS signal can be presented in two ways: showing the intensity on the *z*-axis (Fig. 5a) and presenting an intensity-related colour gradient (Fig. 5b). For presenting depth-resolved measurements, the more applicable is the second type, since this manner of presentation exhibits a more detailed image and is space saving.

A membrane area of 2.4 mm^2 was observed, which consisted of 1025 points. The lateral resolution was 50 μm. In spite of this high resolution, recording of a single image merely required 16 min. Signal amplitudes $\geqslant$3000 indicate the former contact area of the membrane with the donor. However, this region does not exhibit homogeneous PDS signal distribution. The two-dimensional image (Fig. 5b) reveals higher values in the boundary region where the membrane and the edge of the flow-through chamber confined the volume of the cell. This may be attributed to heterogeneous regions in the hoof sample or to the varying flow behaviour at the fringe of the chamber.

According to Eq. (2), a modulation of the excitation frequency permits several layers to be studied, if thermal diffusivity is known.

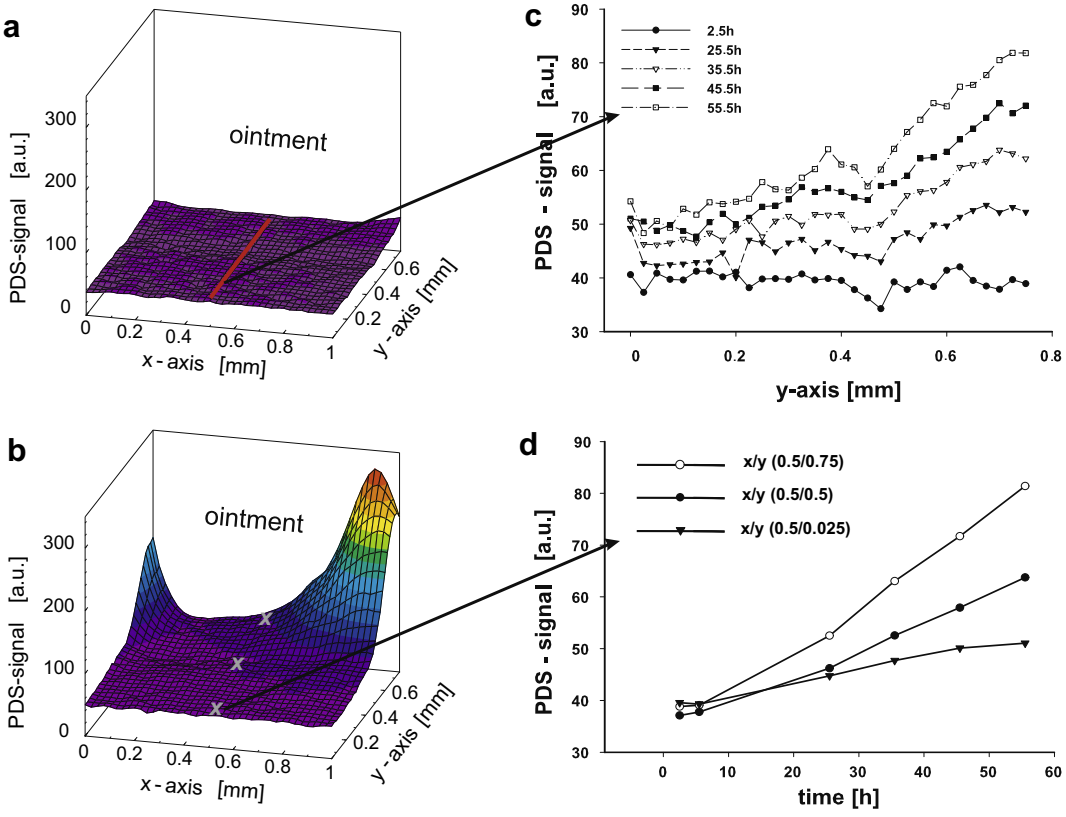

Fig. 4. Imaging of the lateral penetration of dithranol into an artificial DDC membrane. The donor located behind the measurement field consists of a suspension of dithranol in white soft paraffin 10 (w/w%). (a) Displays the measurement after 2.5 h and (b) shows the progress of diffusion process after 55.5 h. The concentration profile of dithranol in the membrane for a single line (at $x = 0.5$ mm) versus time is depicted in (c). The PDS signal–time profile shown for three points of the line (at $x = 0.5$ mm) is presented in (d).

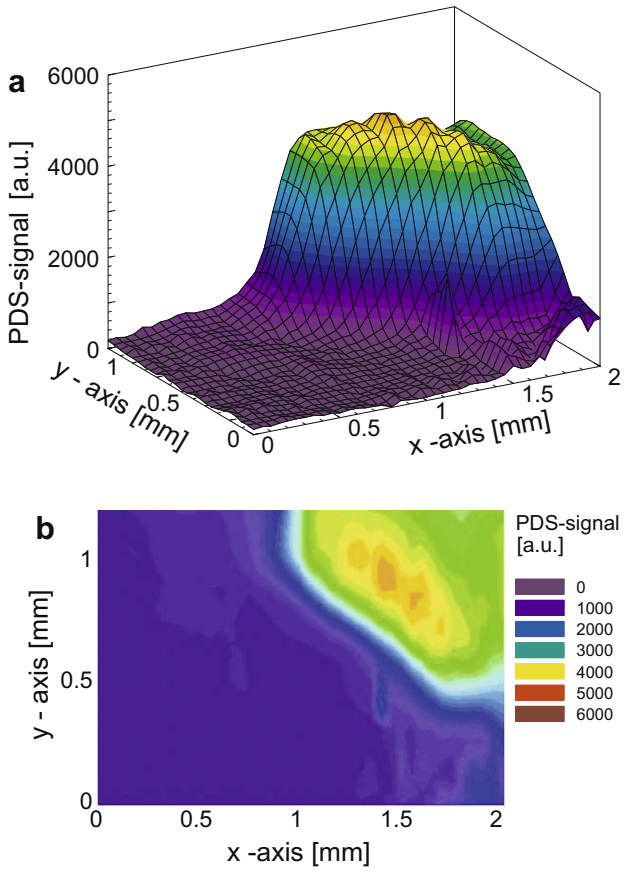

Fig. 5. Types of photothermal visualisation using the 14 Hz PDS imaging of the MO distribution as an example. The *x*-axis and *y*-axis indicate the scanned area. The level of the PDS signal can be presented in two ways: first, the intensity on the *z*-axis is shown (a) and in the second case, the intensity-related colour gradient is presented (b).

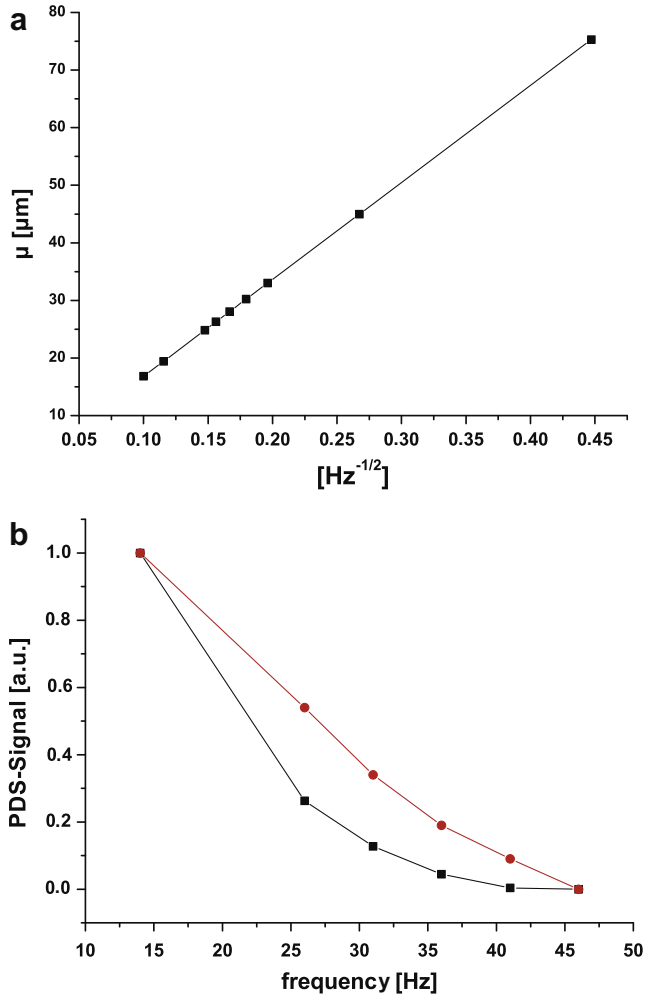

Fig. 6. (a) Thermal diffusion length (μ) is related to the depth of a measurement as being proportional to $\sqrt{\frac{1}{f}}$. A keratin membrane from bovine hoof is used as an example. Thus, various sample depths can be measured by changing the modulation frequency f of the excitation beam. (b) Frequency dependence of the amplitude of the normalised PDS signal data presented for the pure hoof membrane (-♦-) and a membrane part containing MO (-●-).

Dias et al. presented the thermal diffusivity of a human nail to be $\alpha = 8.9 \pm 1.3 * 10^{-4}$ (cm^2/s) [28]. Thus, the structure and physicochemical properties of human nail and bovine hoof are comparable. Therefore, we used these data for the calculation of the thermal diffusion length (μ) of bovine hoof membranes. The linear correlation of the measurement depth with $\sqrt{\frac{1}{f}}$ is shown for a keratin sample in Fig. 6a. Applying the lowest useful modulation frequency of $f = 5$ Hz, Eq. (2) calculates a theoretically maximum thermal diffusion length of 75 μm under the experimental conditions chosen. Indeed, there is not just the correlation of the modulation frequency with the thermal diffusion length. Also, the PDS signal amplitude is increasing at falling modulation frequency. The comparison of a blank membrane with a part of a keratin membrane containing the enriched drug was applied to clarify the origin of the generated signals. The normalised PDS signal amplitudes of both types plotted vs. the modulation frequency exhibit significant difference in developing their curves and do not overlap (Fig. 6b), which demonstrates that our measurements are showing essentially the distributed MO within the membrane. The PDS signal is substantially higher for MO samples than for the untreated sample, and the amplitude is roughly proportional to the MO concentration.

In order to determine the three-dimensional distribution of the MO in the keratin membrane, an area was scanned at various modulation frequencies (Fig. 7). Each frequency corresponds to a certain thermal diffusion length and, hence, to a certain measurement depth (Table 1). Each image in Fig. 7 represents a certain section of the sample, resulting in the three-dimensional visualisation of the MO distribution within the keratin membrane. The MO is detectable at all modulation frequencies. This means that the drug can be found over the depth range from 24 μm to 45 μm. But also outside the saturated region, laterally penetrated MO can be detected. The narrow sections (Fig. 7d and e) are domains, where the drug signals first appeared from 33 μm penetration depth.

The signal-to-noise ratio (S/N) was determined by comparing signals measured in the blank membrane and in the membrane containing MO. Since the pure keratin membrane is highly transparent at the excitation wavelength, this material generates only marginal PDS signals, which we treat as background signals. Therefore, the S/N ratio was calculated from the representative average of PDS signal in the hoof part containing MO and the standard deviation of the background signal. This procedure was applied to all measurements. The results are presented in Table 1. The S/N decreases with rising modulation frequency. At 46 Hz, the signal-to-noise ratio approaches the region of the detection limit ($S/N = 4.8$). Hence, sample sections that are located less than 25 μm away from the surface cannot be measured selectively. On the one hand, the maximum depth is limited by the thermal diffusivity of bovine hoof material, and on the other hand, a minimum measurement depth is required due to the noise arising.

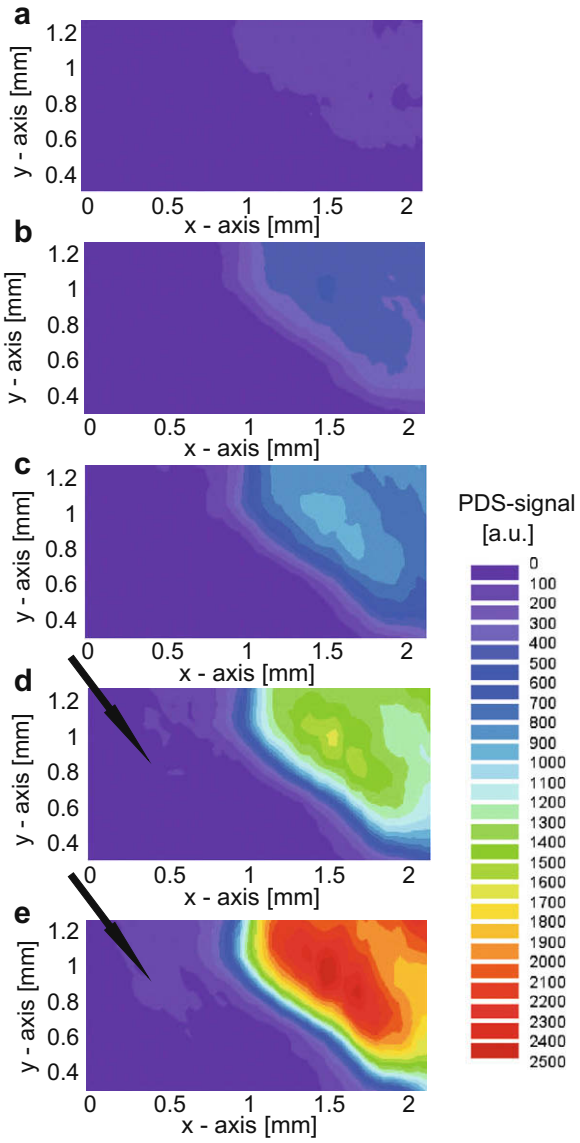

Fig. 7. Depth-resolved PDS imaging of MO distribution in a keratin membrane (thickness 60 μm) for (a) 46 Hz, (b) 41 Hz, (c) 36 Hz, (d) 31 Hz, and (e) 26 Hz (14 Hz measurement is depicted in Fig. 3). The corresponding depth values are presented in Table 1. The arrows in (d) and (e) indicate regions with traces of MO in deeper membrane layers only.

Table 1
Effect of modulation frequency on the measurement depth.

Frequency [Hz]	α (cm^2/s)	μ (cm)	S/N
14	8.9×10^{-4}	4.49×10^{-3}	82.29
26		3.30×10^{-3}	86.15
31		3.02×10^{-3}	74.37
36		2.80×10^{-3}	50.62
41		2.62×10^{-3}	28.11
46		2.48×10^{-3}	4.82

Table 1 shows the thermal diffusion length μ for keratin samples obtained from bovine hoof. μ was calculated by means of Eq. (2) for different modulation frequencies of the excitation beam. Thermal diffusivity is a result of Dias et al. and was measured for human nail samples.
Signal-to-noise ratio (S/N) presented at various modulation frequencies.

When applying PDS imaging for in vivo studies in the future, the safety issue has to be considered. Laser radiation and tissue interact in the photochemical and thermal range. In addition to the wavelength, duration of irradiation, and frequency, the energy density of the laser beam is a critical parameter. The pump beam intensity was evaluated to be 12 W/cm^2 under the experimental conditions selected. A thermographic investigation of the laser-excited pure bovine hoof material revealed that the temperature rise induced in the laser spot was around 2 K (not shown). However, radiation intensities in that range do not induce thermal damage of low absorbing tissue and photochemical reactions are not expected considering the short exposure time of the laser spot on the measurement point.

5. Conclusions

The photothermal deflection spectroscopy and photothermal three-dimensional imaging experiments presented demonstrate the potential of this technique for pharmaceutical and biopharmaceutical use. The drug diffusion process into an artificial membrane was visualised. The preliminary tests carried out by Hanh were extended to dithranol diffusion measurement by means of PDS. The wavelength of the excitation was adapted and the diffusion of DI into the artificial membrane was imaged temporally. During the experiment, lateral diffusion of the drug was found to proceed with a heterogeneous front and could be pursued at a distance of 1 mm from the formulation. The results confirmed Hanh's investigations.

An extraordinary feature of PDS is the non-destructive type of depth measurement. By means of a simple modulation of the excitation beam, various regions of the sample depth can be monitored. The measurement range is limited by the penetration depth of the excitation beam, when opaque samples are investigated. In the case of transparent samples, limitation results from the thermal diffusivity (α) of the sample and, hence, from the thermal diffusion length. For the example of a dry biological keratin membrane from bovine hoof presented, the measurable depth range is between 25 μm and 45 μm, which can be extended in theory to 75 μm. Using the model substance MO, suitability of PDS for three-dimensional imaging of drug distribution in a tissue was demonstrated.

In comparison with FTIR–PAS, which is based on the same principles, PDS shows a lower sensitivity to environmental noise. Hence, PAS does not allow for imaging. PDS is more flexible, since no closed chamber is necessary for measuring. However, PDS is based on the excitation of a sample by monochromatic laser radiation, which constricts the spectrum of applications in comparison to PAS that is based on wide-band excitation. Another method increasingly employed for the investigation of drug penetration process is confocal Raman spectroscopy (CRM). This technique can also be applied to most sample forms and provides imaging in conjunction with depth measurements. However, CRM is also subjected to limitations. CRM is sensitive to stray light, which is why measurements must be carried out in a dark chamber. And the microscope objective has to be positioned close to the surface of the sample, which aggravates in vivo measurements. A further investigation should focus on a comparison of the contactless optical techniques.

In the future, photothermal imaging in conjunction with an appropriate optical double-beam scanner system and depth profiling shall be used to study concentration profiles and kinetics of three-dimensional drug diffusion into skin samples. Later on, in-vivo measurements of the stratum corneum shall be carried out.

Acknowledgement

The author thanks Stefan Heissler for his excellent technical assistance and helpful discussions.

References

[1] J. Hyun Kim, C.H. Lee, H.K. Choi, A method to measure the amount of drug penetrated across the nail plate, Pharmaceut. Res. 18 (10) (2001) 1468–1471.
[2] D. Mertin, B.C. Lippold, In-vitro permeability of the human nail and of a keratin membrane from bovine hooves: prediction of the penetration rate of antimycotics through the nail plate and their efficacy, J. Pharm. Pharmacol. 49 (1997) 866–872.
[3] D. Mertin, B.C. Lippold, In-vitro permeability of the human nail and of a keratin membrane from bovine hooves: penetration of chloramphenicol from lipophilic vehicles and a nail lacquer, J. Pharm. Pharmacol. 49 (1997) 241–245.
[4] K. Moser, K. Kriwet, A. Naik, Y.N. Kalia, R.H. Guy, Passive skin penetration enhancement and its quantification in vitro, Eur. J. Pharm. Biopharm. 52 (2001) 103–112.
[5] B.D. Hanh, R.H.H. Neubert, S. Wartewig, Investigations of drug release from suspensions using FT–ATR technique: part II. Determination of effective dissolution coefficient of drugs, Int. J. Pharm. 204 (2000) 151–158.
[6] B.D. Hanh, R.R.H. Neubert, S. Wartewig, Investigations of drug release from suspensions using FT–ATR technique: part I. Determination of effective diffusion coefficient of drugs, Int. J. Pharm. Sci. 204 (2000) 145–150.
[7] B.D. Hanh, R.H.H. Neubert, S. Wartewig, A. Christ, C. Hentzsch, Drug penetration as studies by noninvasive methods: Fourier transform infrared-attenuated total reflection, Fourier transform infrared, and ultraviolet photoacoustic spectroscopy, J. Pharm. Sci. 89 (9) (2000) 1106–1112.
[8] B.D. Hanh, R.H.H. Neubert, S. Wartewig, J. Lasch, Penetration of compounds through human stratum corneum as studied by Fourier transform infrared photoacoustic spectroscopy, J. Contr. Release. 70 (2001) 393–398.
[9] A. Rosencwaig, E. Pines, Stratum corneum studies with photoacoustic spectroscopy, J. Invest. Dermatol. 69 (1977) 296–298.
[10] H.G.M. Edwards, D.E. Hunt, M.G. Sibley, FT-Raman spectroscopic study of keratotic materials: horn, hoof and tortoiseshell, Spectrochim. Acta A 54 (1998) 745–757.
[11] L. Chrit, P. Bastien, B. Biatry, J.-T. Simonnet, A. Potter, A.M. Minondo, F. Flament, R. Bazin, G.D. Sockalingum, F. Leroy, M. Manfait, C. Hadjur, In vitro and in vivo confocal Raman study of human skin hydration: assessment of a new moisturizing agent, pMPC, Biopolymers 85 (4) (2006) 359–369.
[12] A. Tfayli, O. Piot, F. Pitre, M. Manfait, Follow-up of drug permeation through excised human skin with confocal Raman microspectroscopy, Eur. Biophys. J. 36 (2007) 1049–1058.
[13] P.D.A. Pudney, M. Melot, P.J. Caspers, A. van der Pol, G.J. Puppels, An in vivo confocal Raman study of the delivery of trans-retinol to the skin, Appl. Spec. 61 (8) (2007) 804–811.
[14] P.J. Caspers, G.W. Lucassen, E.A. Carter, H.A. Bruining, G.J. Puppels, In vivo confocal Raman microspectroscopy of the skin noninvasive determination of molecular concentration profiles, J. Invest. Dermatol. 116 (2001) 434–442.
[15] A. Rosencwaig, Photoacousitcs and Photoacoustic Spectroscopy, Robert E. Krieger Publishing Company, 1990.
[16] M. Havaux, L. Lorrain, R.M. Leblanc, Photothermal beam deflection: a new method for in vivo measurements of thermal energy dissipation and photochemical energy conversion in intact leaves, Photosynth. Res. 24 (1990) 63–73.
[17] A. Salnick, W. Faubel, H. Klewe-Nebenius, A. Vendl, H.J. Ache, Photothermal studies of copper patina formed in the atmosphere, Corr. Sci. 37 (1995) 741–767.
[18] R.E. Imhof, A.D. McKendrick, P. Xiao, Thermal emission decay Fourier transform infrared spectroscopy, Rev. Sci. Inst. 66 (11) (1995) 5203–5213.
[19] P. Xiao, J.A. Cowen, R.E. Imhof, In-vivo transdermal drug diffusion depth profiling – a new approach to opto-thermal signal analysis, Anal. Sci. 17 (2001) 349–352.
[20] J.C. Murphy, L.C. Aamodt, Photothermal spectroscopy using optical beam probing: mirage effect, J. Appl. Phys. 51 (9) (1980) 4580–4588.
[21] A.C. Boccara, D. Fournier, J. Badoz, Thermo-optical spectroscopy: detection by the mirage effect, Appl. Phys. Let. 36 (2) (1980) 130–132.
[22] D.O. Lapotko, T.R. Romanovskaya, A. Shnip, V.P. Zahrov, Photothermal time-resolved imaging of living cells, Las. Surg. Med. 31 (2002) 53–63.
[23] V.P. Zharov, D.O. Lapotko, Photothermal imaging of nanoparticles and cells, J. Sel. Top. Quant. Electr. 11 (4) (2005) 733–751.
[24] M. Koebel, M.B. Zimmt, Photothermal readout of surface-arrayed proteins: attomole detection levels with gold nanoparticle visualization, J Phys. Chem. 109 (2005) 16736–16743.
[25] B.D. Hanh, W. Faubel, S. Heissler, S. Wartewig, R.H.H. Neubert, Pharmaceutical applications of photothermal beam deflection, Las. Phys. 16 (5) (2006) 794–798.
[26] L.C. Aamodt, J.C. Murphy, Photothermal measurements using a localized excitation source, J. Appl. Phys. 52 (8) (1981) 4903–4914.
[27] R.H.H. Neubert, C. Bendas, W. Wohlrab, B. Gienau, W. Fürst, A multilayer membrane system for modelling drug penetration into skin, Int. J. Pharm. Sci. 75 (1991) 89–94.
[28] D.T. Dias, L.E.R. Nuglish, E. Sehn, M.L. Baesso, A.N. Medina, A.C. Bento, Human nail thermal diffusivity obtained using the open photoacoustic cell technique, J. Phys. IV 125 (2005) 657–660.